Chemical Physics Letters 771 (2021) 138493

Contents lists available at ScienceDirect

Chemical Physics Letters

journal homepage: www.elsevier.com/locate/cplett

Research paper

Temperature dependence of the rate coefficient of formation of CN radical from C + NH

Ernesto Garcia [a,*], Alexandre Zanchet [b,c], F. Javier Aoiz [b]

[a] Departamento de Quimica Fisica, Universidad del Pais Vasco (UPV/EHU), Vitoria 01006, Spain
[b] Departamento de Quimica Fisica (Unidad asociada CSIC), Universidad Complutense, Madrid 28008, Spain
[c] Instituto de Fisica Fundamental, CSIC, Madrid 28008, Spain

A B S T R A C T

Rate coefficients of the complex-forming C + NH→H + CN reaction have been calculated at temperatures ranging from 5 K to 800 K using quasi-classical trajectories on a potential energy surface which accurately describes the attractive long-range interaction, along with results using two capture models. In contrast with the constant value recommended in astrochemical databases, a steep decrease of the rates has been found up to 150 K, and then they tends to be nearly constant. Such behavior is analyzed in terms of the rovibrational state-selected rate coefficients and cross sections singling out the role played by the rotational excitation of the initial diatom. The effect of the electronic degeneracy is also discussed.

1. Introduction

The reaction between the carbon atom (C) and the imidogen radical (NH) to form the hydrogen atom (H) and the cyano radical (CN), C + NH → H + CN, involves chemical species of relevance in astrochemistry [1]. In particular, the cyano radical (the second molecule to be identified in the interstellar space [2]) is one of the most widely spread molecules, and is very reactive with hydrocarbons even at very low temperatures [3]. Moreover, the formed organic molecules with the –CN group are considered as a source of pre-biotic amino-acids. Additionally, the reaction can proceed through either the hydrogen cyanide (HCN) or the hydrogen isocyanide (HNC), which are also widespread astromolecules.

Main astrochemical databases (KIDA [4], UdFA [5]) recommend for the rate coefficient of the mentioned reaction a constant value of $1.20\cdot 10^{-10}$ cm^3 s^{-1} for temperature values ranging from 10 to 300 K. However, this is an estimated value because, to our knowledge, there are neither experimental nor theoretical kinetic data available.

An accurate potential energy surface (PES) for the $X^1\Sigma^+$ ground-state of the triatomic HCN system was published by Varandas and Rodrigues [6,7]. This PES is based in a fit of accurate ab initio data by using the Double-Many Body Expansion methodology (DMBE) [8–10]. The HCN ($X^1\Sigma^+$) DMBE PES correlates with the following products:

$$\begin{aligned} \mathrm{HCN}(X^1\Sigma^+) \rightarrow\ & \mathrm{H}(^2S) + \mathrm{CN}(X^2\Sigma^+) \quad D_e = 132.6\,\mathrm{kcal\,mol^{-1}} \\ \rightarrow\ & \mathrm{C}(^3P) + \mathrm{NH}(X^3\Sigma^-) \quad D_e = 231.6\,\mathrm{kcal\,mol^{-1}} \\ \rightarrow\ & \mathrm{N}(^4S) + \mathrm{CH}(a^4\Sigma^-) \quad D_e = 247.9\,\mathrm{kcal\,mol^{-1}} \\ \rightarrow\ & \mathrm{N}(^4S) + \mathrm{C}(^3P) + \mathrm{H}(^2S) \quad D_e = 313.3\,\mathrm{kcal\,mol^{-1}} \end{aligned}$$

Note that the DMBE PES does not correlate with the N(^4S) + CH($X^2\Pi$) channel, *i.e.*, with the electronic ground-states of N and CH, and therefore that reaction cannot be studied adiabatically on the DMBE PES. That channel correlates with the $1^3A'$ and $1^3A''$ surfaces of HCN [11].

In this work the study of the reaction makes use of the ground-state $1^1A'$ DMBE PES that correlates with the HCN($X^1\Sigma^+$) molecule as intermediate:

$$\mathrm{C}(^3P) + \mathrm{NH}(X^3\Sigma^-) \rightarrow \mathrm{H}(^2S) + \mathrm{CN}(X^2\Sigma^+) \quad \Delta D_e = -99.0\,\mathrm{kcal\,mol^{-1}} \qquad (1)$$

The reactants give rise to a series of singlet and triplet A', A' and A'' PESs, while the products correlate with singlet and triplet A' PESs. However, only the $1^1A'$ PES correlates adiabatically with the HCN($X^1\Sigma^+$) intermediate.

When the zero-point energy of both reactant and product diatoms is included, reaction 1 becomes exothermic by $\Delta_r H_0^0 = -100.7$ kcal mol^{-1}. The other possible product channel, N(^4S) + CH($a^4\Sigma^-$), is of scarce interest in astrochemistry studies due to its endoergicity of 16.3 kcal mol^{-1}.

Reaction 1 on the DMBE PES is characterized by an attractive long-

* Corresponding author.
E-mail address: e.garcia@ehu.es (E. Garcia).

https://doi.org/10.1016/j.cplett.2021.138493
Received 13 December 2020; Received in revised form 18 February 2021; Accepted 24 February 2021
Available online 10 March 2021

range tail of the interaction between reactants when the carbon atom approaches the N end of the diatom ($\gamma = 180^{\circ}$), whereas a barrier arises when the attack takes place from the H side. A further approach between reactants leads to the very deep well corresponding to HCN (and also HNC, 17.4 kcal mol^{-1} higher in energy and separated from the HCN well by a transition state of 47.5 kcal mol^{-1}). Then the potential energy increases smoothly along the exit channel to products.

It should be emphasized here that the $1^1A'$ DMBE PES describes accurately the long-range potential energy. In fact, different functional forms are used to represent the short- and long-range interactions. The inner part of the PES is described with a polynomial of the three internuclear distances (whose coefficients are obtained by fitting rovibrational spectroscopic data and ab initio energies) and it is damped as the internuclear distances increase. The long-range energy includes both the dispersion and the electrostatic energies. The internuclear and angular dependence of the dispersion coefficients has been estimated using the dipolar isotropic and anisotropic polarizabilities of fragments while the electrostatic potential has been formulated in terms of the interaction of the quadrupole moment of carbon with the dipole and quadrupole moments of NH. Such expression of the long-range energy is based on an atom–atom interaction, in contrast with the description of the interaction as a sum of atom-bond contributions formulated by F. Pirani [12,13].

The goal of the present work is to study the dependence of the rate coefficients on the temperature for reaction 1 in a range of interest for astrochemistry. To this end, we have studied the kinetics and the dynamics of this reaction driven by long-range forces which are realistically described by the accurate DMBE PES. This Letter is laid out as follows: Section 2 describes the theoretical approaches; Section 3 is devoted to the analysis of the calculated rate coefficients and of their dependence on the temperature. Section 4 extends the analysis to state-selected cross sections and rate coefficients. Conclusions are drawn in Section 5.

2. Theoretical methodology

The huge number of rovibrational states involved in the investigated processes (associated with the deep HCN potential well and the significant exoergicity of the reaction channel) prevents the use of quantum dynamical methodologies. Accordingly, the quasi-classical trajectory (QCT) method [14,15] is the most convenient methodology to study reaction 1. As a matter of fact, the QCT treatment is extensively used in astrochemical investigations (see, for example, Refs. [16–32]). In addition to QCT techniques, some attempts to investigate complex-forming reactions have been made using the RPMD (Ring Polymer Molecular Dynamics) method [33–42].

In this work, QCT calculations were carried out using the program VENUS96 [43] on the DMBE PES, whose derivatives were computed numerically. Two series of QCT calculations were performed to determine thermal rate coefficients and, separately, state-selected cross sections. The QCT thermal rate coefficient $k(T)$ is written as:

$$k\left(T\right) = g_e\left(T\right)\left(\frac{8k_BT}{\pi\mu}\right)^{1/2}\pi\, b_{max}^2\,\frac{N_r}{N} \tag{2}$$

where $g_e(T)$ is the electronic degeneracy factor, k_B the Boltzmann's constant, μ the reduced mass of the reactants, b_{max} is the maximum value of the impact parameter leading to reaction and N_r is the number of reactive events out of the total number of integrated trajectories N. On each trajectory, the collision energy is selected according to the Maxwell-Boltzmann distribution at temperature T and the initial rovibrational state of the diatom is also sampled according to a Boltzmann distribution for temperature T over the manifold of states supported by the diatomic potential curve.

The electronic factor is calculated considering that the reaction takes place only on the ground $1^1A'$ PES, and the C atom partition function accounting for the ground state spin–orbit splitting is:

$$g_e\left(T\right) = \frac{1}{1 + 3\exp(-E_{J=1}/k_BT) + 5\exp(-E_{J=2}/k_BT)} \tag{3}$$

where $E_{J=1} = 16.4$ cm^{-1} and $E_{J=2} = 43.4$ cm^{-1} are the energies of the $J = 1$ and $J = 2$ states of the ground triplet term ($^3P_{0,1,2}$) of the C atom, referred to the energy of the $J = 0$ spin–orbit ground state [44]. The value of g_e converges to 1/9 at high temperatures, but it increases as the temperature decreases ($g_e = 0.17$ at 100 K and $g_e = 0.77$ at 10 K).

Thermal rate coefficients were calculated at 27 temperature values ranging from 5 K to 800 K, with a finer grid for lower temperatures. A total of $N = 10^6$ trajectories were integrated at each of the considered temperatures, leading to a standard deviation of the rate coefficient lower than 0.5%.

To rationalize the thermal rate coefficient $k(T)$, we calculated the rovibrational state-selected cross sections $\sigma(E_{tr}; v, j)$ using:

$$\sigma\left(E_{tr}; v, j\right) = \pi\, b_{max}^2\,\frac{N_r(E_{tr}; v, j)}{N(E_{tr}; v, j)} \tag{4}$$

where $N_r(E_{tr}; v, j)$ is the reactive subset of the total number of integrated trajectories $N(E_{tr}; v, j)$ generated with a given collision energy E_{tr} at a given rovibrational state of NH characterized by the quantum numbers v and j. By integrating the cross sections $\sigma(E_{tr}; v, j)$ over the Maxwell–Boltzmann distribution of the collision energy E_{tr} at a given temperature T, the rovibrational state-selected rate coefficients $k(T; v, j)$ can also be worked out.

State-selected cross sections were calculated at 56 collision energy values in the $1{\cdot}10^{-3}$ – 5 kcal mol^{-1} range, with a finer grid at lower energies. The rovibrational states of NH considered were $v = 0$ and $j = 0, 1, 2, 3, 4$ to investigate the effect of the rotational excitation on the cross section. Some additional calculations were carried out also for $v = 1$ and $j = 0$. The number of integrated trajectories ranges from $N = 2{\cdot}10^4$ at the highest energies (and lower maximum impact parameter, see below) to $N = 10^5$ for the lowest energies. Overall, the standard deviation of the cross section is less than 1%. To calculate the rovibrational state-selected rate coefficients $k(T; v, j)$ out of the corresponding cross sections, a cubic-spline interpolation and extrapolation of their values was first performed. The temperatures considered range from 5 K to 245 K.

The long-range interaction between reactants extends to large distances. For this reason, both the initial distance to start the trajectory integration and the integration step were selected synchronically. Effectively, an initial distance of 34 Å and an integration step of 0.1 fs guarantee both an interaction energy between the reactants and an average conservation of the total energy of about $4{\cdot}10^{-4}$ kcal mol^{-1} (with an integration step of 0.05 fs the total energy conservation can be improved by two orders of magnitude, while the rate coefficient at 10 K is modified only of 0.04%). The final separation of product fragments was instead set shorter (21 Å) because the H + CN interaction energy at that distance is smaller than $1{\cdot}10^{-5}$ kcal mol^{-1}.

The selection of the maximum impact parameter leading to reaction is also dictated by the attractive nature of the long-range interaction. Such an attractive nature of the long-range interaction implies that collisions with a large value of the impact parameter can fall into the deep HCN well and then form the products. We set b_{max} equal to the value of the impact parameter leading to a N_r/N probability lower than the 0.2%. This criterion returns b_{max} values highly depending on both temperature and collision energy. Thus, the maximum impact parameter decreases from 27 Å to 8 Å as the temperature increases from $T = 5$ K to 800 K, while it decreases from 26 Å to 4 Å as the collision energy increases from $E_{tr} = 1{\cdot}10^{-3}$ to 5 kcal mol^{-1}. Once selected the value of b_{max} at a given energy, the impact parameter for each trajectory was chosen randomly according to the function $b_{max}\mathscr{R}^{1/2}$, with $\mathscr{R}$ being a random number $\mathscr{R} \in [0, 1]$.

As already mentioned, reaction 1 is a complex-forming collision driven by the long-range interaction. This characteristic suggested us to apply a capture model to work out an approximate estimate of the cross sections and rate coefficients [45]. In this work, two simple capture models were adopted in order to investigate whether the long-range forces can suitably describe the dynamics and kinetics of reaction 1.

The first model (model 1) takes into account the main long-range force, the interaction between the electric dipole moment of the molecule and the induced dipole of the atom, which can be described in SI units by [46]:

$$V^{(\text{model1})}\left(R\right) = -\frac{\alpha_{\text{el}}^{'}\, p^2}{\left(4\,\pi\,\epsilon_0\right)^2 R^6} = -\frac{\alpha_{\text{el}}\, p^2}{\left(4\,\pi\,\epsilon_0\right) R^6} = -\frac{C_6}{R^6} \tag{5}$$

where $\alpha_{\text{el}}^{'}$ is the electric polarizability of the carbon atom ($1.858{\cdot}10^{-40}$ $\text{J}^{-1}\,\text{C}^2\,\text{m}^2$) and $\alpha_{\text{el}} = \alpha_{\text{el}}^{'}/(4\pi\epsilon_0) = 1.670$ Å^3 [47]), p is the electric dipole moment of the imidogen radical ($4.653{\cdot}10^{-30}$ C m = 1.395 D) [48]) and ϵ_0 is the permittivity of vacuum. Hence the C_6 coefficient has a value of 46.78 kcal mol^{-1} Å^6. Fig. 1 shows the interaction formulated in Eq. (5) as a function of the Jacobi coordinate R (the distance between the atom and the center-of-mass of the molecule). As apparent from the Figure, the bare dipole–induced dipole interaction is quite weak.

Assuming a barrier-less reaction and a long-range interaction as that given by Eq. (5), the dependence of the cross section σ on the translational energy E_{tr} is given by [45]:

$$\sigma^{(\text{model1})}\left(E_{\text{tr}}\right) = 3\,\pi\left(\frac{C_6}{4\,E_{\text{tr}}}\right)^{1/3} \tag{6}$$

that leads to the following dependence of the rate coefficient k on the temperature T:

$$k^{(\text{model1})}\left(T\right) = 3\left(2^{5/6}\right)\sqrt{\frac{\pi}{\mu}}\,\Gamma\left(\frac{5}{3}\right)\left(C_6^2\,k_{\text{B}}\,T\right)^{1/6} \tag{7}$$

where Γ is the gamma function, μ is the reduced mass of the reactants, and k_{B} is the Boltzmann constant. As is shown by Eq. (7), the capture model with a dipole – induced dipole interaction describes an increase of the rate coefficient as the temperature increases.

The second model (model 2) is based on the long-range potential given by the DMBE PES, which takes into account more interactions than the bare dipole–induced dipole one, as already mentioned. Moreover, the long-range potential energy of DMBE PES depends on the angle between the atom and the molecule. As can be seen in Fig. 1, where the long-range energy of DMBE PES is shown as a function of R for several values of the angle γ (the C –NH Jacobi angle between $\boldsymbol{R}$ and the NH internuclear vector, $\boldsymbol{r}$) and fixing the molecule in its equilibrium distance, the most favorable atom-molecule approach occurs at $\gamma = 180^\circ$ (*i.e.*, when of the C atom heads on the N atom of the molecule) and the attractive interaction extends to the perpendicular approach. In contrast, when the C atom approaches the H side of the molecule ($\gamma = 0^\circ$), the interaction is attractive at long distances ($R \geq 4.2$ Å) to become repulsive at smaller distances. To get a global, isotropic potential, the orientation-averaged potential was calculated. To this end, the potential energy is formulated as an expansion in terms of Legendre polynomials [45]:

$$V^{(\text{model2})}\left(R,\gamma\right) = \sum V_\lambda\left(R\right) P_\lambda\left(\cos\gamma\right) \tag{8}$$

(note that the dependence on the internuclear distance of the molecule is dropped since only its equilibrium value is considered), and the orientation-averaged potential can be calculated by integrating over the angle γ:

$$V_0\left(R\right) = \frac{1}{2}\int_0^\pi V^{(\text{model2})}\left(R,\gamma\right)\sin\gamma\,\text{d}\gamma \tag{9}$$

Accordingly, V_0 represents the isotropic term of the expansion, which is purely attractive for $R \gtrsim 3.1$ Å, as shown in Fig. 1.

In models 1 and 2, it is assumed that the reaction probability is unity when the atom-molecule collision has sufficient translational energy to overcome the energy barrier (only the centrifugal barrier for attractive long-range interaction) and, consequently, the capture of the atom by the molecule occurs by forming a three-atom complex. Accordingly, the reaction cross section at the given translational energy is simply the area of the circle with the largest impact parameter for which the translational energy exceeds the centrifugal barrier, *i.e.* $\sigma(E_{\text{tr}}) = \pi b_{\text{c}}^2$. The value of b_{c} is the solution of the implicit equation [45]:

$$E_{\text{tr}} = V_0\left(R_{\text{max}}\right) + \frac{E_{\text{tr}}\,b_{\text{c}}^2}{R_{\text{max}}^2} \tag{10}$$

where R_{max} is the location of the centrifugal barrier maximum at given translational energy and impact parameter. In the last step, the reaction rate coefficient is obtained by integrating the cross section over the translational energy at the required temperature T.

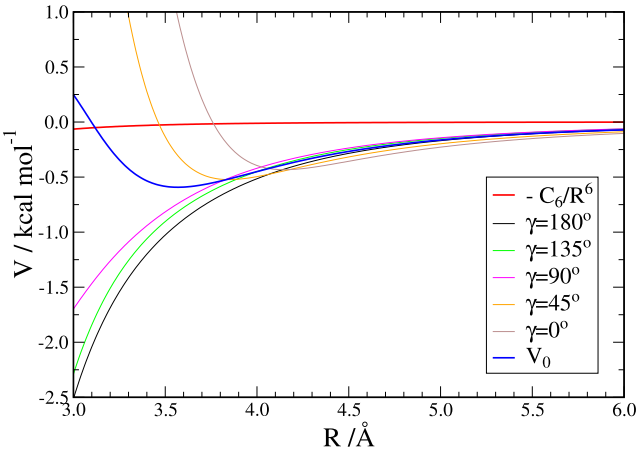

Fig. 1. Long-range potential energy of the dipole – induced dipole interaction ($-C_6/R^6$), of the DMBE PES for different values of the $\widehat{\text{CNH}}$ angle (γ) and the calculated orientation-averaged potential (V_0) plotted as a function of the distance R.

3. Rate coefficients

The QCT thermal rate coefficient computed without including the electronic factor is shown in Fig. 2 as a function of the temperature T. It is evident from the Figure that there is a dependence of the QCT rate coefficient on the temperature, even when the temperature dependent electronic degeneracy factor, g_e, is not included (see below). In fact, the rate coefficient increases from 5 K to 10 K and then it decreases smoothly as the temperature further increases. Fig. 2 displays also the rate coefficients calculated using the two capture models previously described, also without including the electronic factor. The rate coefficients obtained using "model 1" (calculated with Eq. (7)) show a sharp increase with the temperature at the lower T values and a smoother one at higher T. When using "model 2", a similar temperature dependence of $k(T)$ is found though with larger absolute values due to the stronger long-range attractive potential used in "model 2" (as shown in Fig. 1). However, Fig. 2 provides a clear evidence that the two capture models describe a dependence of the rate coefficient with the temperature opposite to the one obtained from QCT calculations.

The dependence of the rate coefficient of reaction 1 with the temperature, displayed in Fig. 2, changes drastically when the electronic factor g_e of Eq. (3) is taken into account. As shown in Fig. 3, at low temperature all the curves fall sharply as a consequence of the

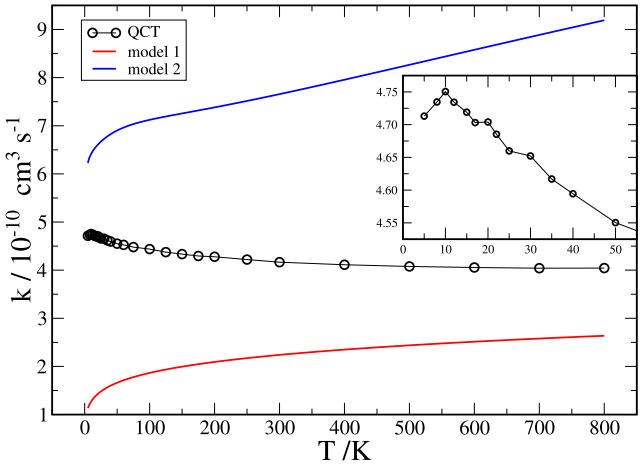

Fig. 2. QCT values of the thermal rate coefficient for the C + NH → H + CN reaction plotted as a function of the temperature T. Error bars are smaller than the size of the circles used in the Figure. The rate coefficients obtained from the capture models are also shown. The inset shows the QCT values at low temperatures.

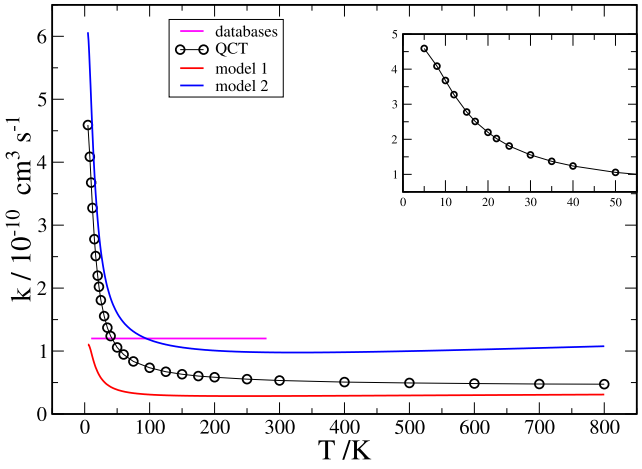

Fig. 3. QCT values of the thermal rate coefficient for the C + NH → H + CN reaction including the electronic factor of Eq. (3) plotted as a function of the temperature T. The rate coefficient recommended in the astrochemical databases and the rate coefficients obtained from the capture models including the electronic factor are also shown. The inset shows the QCT values at l.ow temperatures.

substantial decrease of the value of g_e as T increases. The QCT $k(T)$, as well as those of models 1 and 2, decrease abruptly up to $T = 150$ K before becoming nearly constant up to the highest temperature value calculated in this work. Fig. 3 also shows the constant value of the rate coefficient recommended in the astrochemical databases for reaction 1 for temperatures ranging from 10 K to 300 K, in contrast with the values given by the QCT calculations and the two model predictions. However, above $T = 200$ K the QCT is practically constant ($\sim 6{\cdot}10^{-11}$) as well as the predictions of "model 1" ($\sim 3.5{\cdot}10^{-11}$) and "model 2" ($\sim 1.1{\cdot}10^{-10}$). The value recommended by astrochemical databases ($1.2{\cdot}10^{-10}$) lies slightly above the latter value and coincides with the QCT one computed at $T = 50$ K.

Most often, the dependence on the temperature of the rate coefficient of bimolecular reactions is parametrized in the astrochemical databases using the Arrhenius-Kooij formula [49]:

$$k\left(T\right) = \alpha \left(\frac{T}{300}\right)^{\beta} \exp\left[-\frac{\gamma}{T}\right] \tag{11}$$

However, this expression is not adequate to fit the sharp decrease at $T < 50$ K and the subsequent levelling off. In order to maintain the widely used and convenient function of Eq. (11), we propose to modified it as follows:

$$k_{\text{fit}}\left(T\right) = g_e\left(T\right) \alpha \left(\frac{T}{300}\right)^{\beta} \exp\left[-\frac{\gamma}{T}\right] \tag{12}$$

where the electronic factor is given by Eq. (3). The best-fit parameters of the logarithmic expression of Eq. (11) with the calculated QCT rate coefficients without the electronic factor are $\alpha = 4.20{\cdot}10^{-10}$ cm^3 s^{-1}, $\beta = -0.049$ and $\gamma = 0.448$ K, with a χ^2 of $6.3{\cdot}10^{-24}$ and a correlation-coefficient of 0.9983. As shown in Fig. 4, the parametrized function well describes the calculated QCT rate coefficients at the lower temperatures.

4. Cross sections

The most detailed quantity reported in the present work is the excitation function of the C + NH → H + CN reaction for several NH rovibrational states. QCT estimates of the state-selected cross sections computed for the mentioned initial (v,j) states are plotted for comparison in Fig. 5 by ignoring the electronic factor for a clearer comparison of the QCT total rate coefficients and the initial state-selected ones. As is apparent in the Figure, the cross section curve is the one typical of barrier-less reactions: very large at low collision energy, sharply decreasing as the energy increases, and mildly decreasing for a further increase of the collision energy. Over this pattern, there are clear differences depending on the rotational excitation. At low collision energies (see upper panels of Fig. 5), the excitation functions for different rotational states are almost parallel. However, the rotational excitation causes some differences in intermediate values of the collision energy (see the bottom left panel of Fig. 5). In particular, it is worth noting that the absence of rotational energy in the initial diatom makes the cross sections smaller than those obtained when the initial diatom is rotationally excited. At the higher collision energies considered here (see lower right panel of Fig. 5) the values of $\sigma(E_{\text{tr}}; v, j)$ for all the initial rotational energies differ negligibly.

The panels of Fig. 5 also show the excitation functions calculated using the two capture models. Both exhibit large values of the cross sections at the lowest collision energy, a significant decrease as the collision energy just increases and a milder decline at the higher energies. However, the "model 1" curve is always lower than all the QCT curves whereas the "model 2" one is always higher.

As already mentioned, "model 2" estimates the cross section at a given translational energy as $\sigma(E_{\text{tr}}) = \pi b_c^2$, assuming that the capture

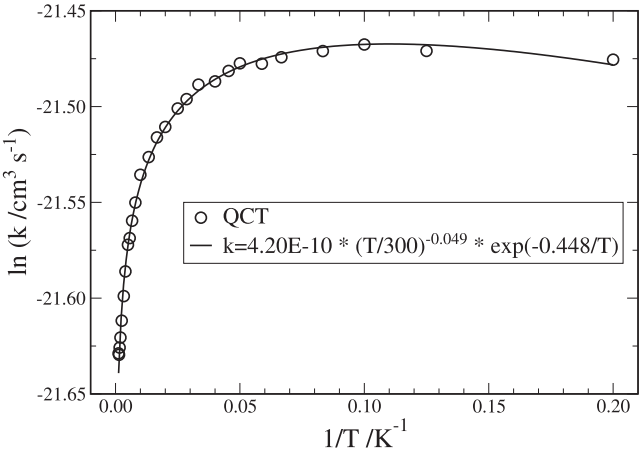

Fig. 4. Arrhenius plot of the QCT values of the thermal rate coefficient $k(T)$ and of the Arrhenius-Kooij best-fitting curve.

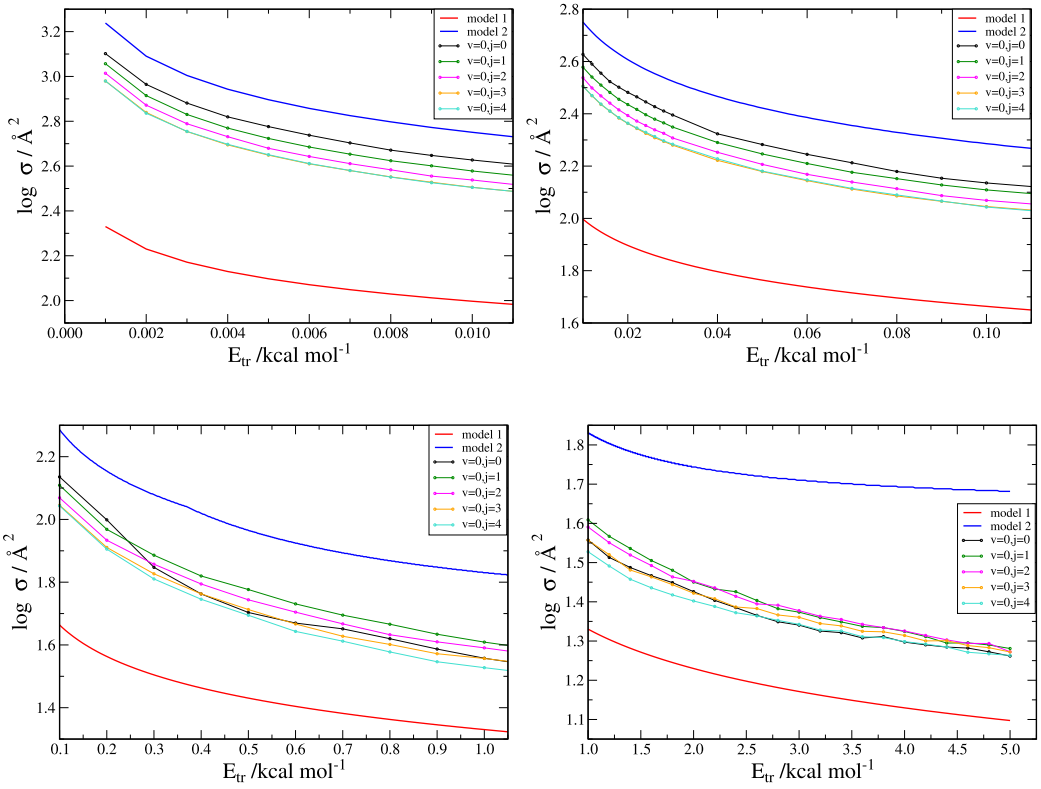

Fig. 5. QCT values of the state-selected cross section for the C + NH → H + CN reaction plotted as a function of the translational energy E_{tr}. Each panel shows a different range of values of E_{tr}.

probability to form the three-atom complex is unity. When the dependence of the maximum impact parameter b_c on the translational energy is compared with the dependence of the maximum impact parameter b_{max} obtained from QCT calculations, it is found that they are very similar at all collision energies (for instance, at $E_{tr} = 1.0$ kcal mol^{-1} $b_{max} = 4.7$ Å for "model 2" and 4.8 −5.0 for QCT). This indicates that the maximum impact parameter selected in the trajectory method is close to the centrifugal barrier along the long-range attractive interaction. However, in spite of the similar value of the maximum impact parameters, the cross sections from "model 2" are significantly larger than those obtained from QCT calculations (see Fig. 5). This implies that the two assumptions relating to "model 2" are not fulfilled. Namely, the potential cannot be considered isotropic (the reaction is hindered for some atom–diatom approaches), and the assumption that the capture probability is one for all impact parameters below its maximum value is not supported by the classical dynamics of the reaction.

QCT cross sections averaged over the Maxwell–Boltzmann distribution of collision energy render the rovibrational state-selected rate coefficients $k(T;v,j)$, which provide some more insight into the kinetics of reaction 1. The resulting values of $k(T;v,j)$ for $v = 0$ and $j = 0, 1, 2, 3, 4$ are shown in Fig. 6 together with the thermal values. From the Figure, it is apparent that the dependence on the temperature of the state-selected rate coefficients is very sensitive to the initial rotational diatom state. When the initial diatom is in its ground rovibrational state, the rate coefficient exhibits a broad maximum at 30 K and decreases when increasing T. In contrast, the rotational excitation of the diatom leads to an increase of the rate as the temperature increases and to a flattening for further temperature increases. This dependence on the temperature is qualitatively similar to that of the thermal rate coefficients for capture models (see Fig. 2), and can be explained assuming that, when NH rotates, the C atom observes an orientation-averaged long-range attraction.

Moreover, as shown in the Figure, the larger the rotational excitation, the lower the value of the rate coefficient, with $k(T;v = 0,j = 3)$ and $k(T;v = 0,j = 4)$ being almost coincident at low temperature. The value of the thermal rate coefficient at $T = 10$ K coincides with the $j = 0$ term. However, at higher temperatures the contribution from $j = 1$ becomes important (for example, at 30 K it amounts to 36%) resulting in a decrease of the thermal rate coefficient. This explains why the maximum of the thermal rate coefficient is located at 10 K, while that of $k(T;v = 0, j = 0)$ occurs at 30 K. As the temperature increases further (say, at 100 K), the thermal rate keeps decreasing as a result of both the decrease of the $j = 0$ rate and the contribution from the lower $k(T;v = 0,j = 2)$ and $k(T;v = 0,j = 3)$ (25% and 8%, respectively) with the main contribution at that temperature coming from $j = 1$.

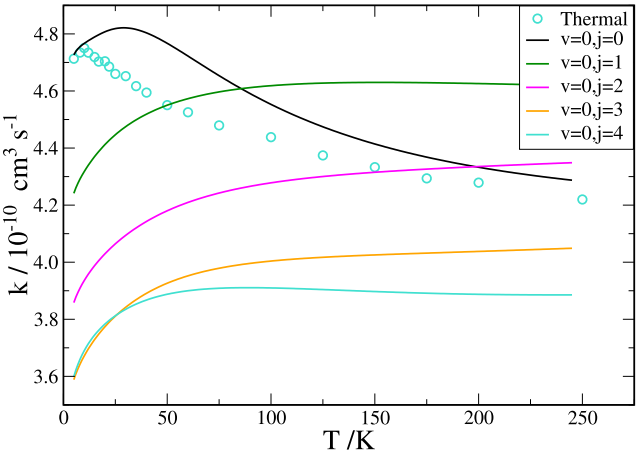

Fig. 6. QCT values of the thermal and state-selected rate coefficient for the C + NH → H + CN reaction plotted as a function of the temperature T.

5. Conclusions

The rate coefficient recommended for reaction 1 in the astrochemical databases is a temperature-independent empirical estimate. A more educated attempt to calculate the temperature dependence of such rate coefficient is the use of capture models. This is, in principle, adequate for this reaction that is dominated by a long-range attractive interaction leading to the formation of a relatively long-lived complex. To this end, two capture models have been proposed in this work: "model 1" based on a simple dipole–induced dipole interaction, and "model 2" using a more sophisticate long-range potential derived from the accurate DMBE PES, averaged over all approaching angles. When the electronic degeneracy factor is ignored, the value of the rate coefficients computed using both models show a smooth increase with temperature (though those from "model 2" results to be noticeably larger than those from "model 1" as a consequence of a stronger interaction). However, when the electronic factor is included, both models predict an abrupt decrease of the rate coefficient up to $T = 150$ K with a levelling-off at higher temperatures. An improved way to treat the kinetics, and still computationally affordable, is to deal with the overall PES, as the QCT method does. When the electronic factor is included, the QCT rate coefficients are respectively larger and smaller than those obtained with "model 1" and "model 2". With respect to the recommended value in the databases, the QCT value is higher below 50 K, but at higher T values it becomes smaller by a factor of 2.

In order to investigate the discrepancies between the capture model and the QCT results, the QCT rovibrational state-selected cross sections were calculated for several internal states of the initial molecule on a wide range of collision energy values. In all cases, the excitation functions reveal the typical behavior of barrier-less reactions with large cross section values at low energies. The dependence of the curves on the initial rotational excitation has allowed us to rationalize the decrease of the rate coefficient with temperature. However, what is interesting to remark here is that the maximum impact parameters in "model 2' and in the QCT calculations practically coincide and, consequently, the discrepancies in the cross sections can be attributed to the intrinsic assumptions of the capture models.

Declaration of Competing Interest

None.

Acknowledgment

We thank Prof. A.J.C. Varandas for making available to us the DMBE potential energy surface and the Oklahoma University Supercomputing Center for Education & Research (OSCER) and the European Grid Infrastructure (EGI) through COMPCHEM Virtual Organization for providing computing resources and services. The authors also acknowledge the financial support from the MINECO/FEDER of Spain under grants PGC2018-096444-B-I00, PID2019-107115 GB-C21 and FIS2017-83473-C2.

References

[1] B.A. McGuire, Astrophys. J., Suppl. Ser. 239 (2018) 17, https://doi.org/10.3847/1538-4365/aae5d2.
[2] A. McKellar, Publ. Astron. Soc. Pac. 52 (1940) 187, https://doi.org/10.1086/125159.
[3] I.R. Sims, J.-L. Queffelec, D. Travers, B.R. Rowe, L.B. Herbert, J. Karthauser, I. W. Smith, Chem. Phys. Lett. 211 (1993) 461–468, https://doi.org/10.1016/0009-2614(93)87091-G.
[4] V. Wakelam, et al., Astrophys. J. Suppl. Ser. 199 (2012) 21, https://doi.org/10.1088/0067-0049/199/1/21.
[5] D. McElroy, C. Walsh, A.J. Markwick, M.A. Cordiner, K. Smith, T.J. Millar, Astron. Astrophys. 550 (2013) A36, https://doi.org/10.1051/0004-6361/201220465.
[6] A.J.C. Varandas, S.P.J. Rodrigues, J. Chem. Phys. 106 (1997) 9647–9658, https://doi.org/10.1063/1.473864.
[7] A.J.C. Varandas, S.P.J. Rodrigues, J. Phys. Chem. A 110 (2006) 485–493, https://doi.org/10.1021/jp051434p.
[8] A.J.C. Varandas, Adv. Chem. Phys. 74 (1988) 255–338, https://doi.org/10.1002/9780470141236.ch2.
[9] A. Varandas, Chem. Phys. Lett. 194 (1992) 333–340, https://doi.org/10.1016/0009-2614(92)86060-U.
[10] A.J.C. Varandas, in: A. Laganà, A. Riganelli (Eds.), Reaction and Molecular Dynamics, volume 75 of Lect. Notes in Chemistry, Springer, 2000, pp. 33–56.
[11] J. Daranlot, et al., Phys. Chem. Chem. Phys. 15 (2013) 13888–13896, https://doi.org/10.1039/C3CP52535J.
[12] F. Pirani, D. Cappelletti, G. Liuti, Chem. Phys. Lett. 350 (2001) 286–296, https://doi.org/10.1016/S0009-2614(01)01297-0.
[13] F. Pirani, M. Albertí, A. Castro, M. Moix Teixidor, D. Cappelletti, Chem. Phys. Lett. 394 (2004) 37–44, https://doi.org/10.1016/j.cplett.2004.06.100.
[14] M. Karplus, R.N. Porter, R.D. Sharma, J. Chem. Phys. 43 (1965) 3259–3287, https://doi.org/10.1063/1.1697301.
[15] D.G. Truhlar, J.T. Muckerman, in: R.B. Bernstein (Ed.), Atom-Molecule Collision Theory, Springer, US, 1979, pp. 505–566.
[16] F.J. Aoiz, T. González-Lezana, V. Sáez-Rábanos, J. Chem. Phys. 129 (2008) 094305, https://doi.org/10.1063/1.2969812.
[17] S. Joseph, P.J.S.B. Caridade, A.J.C. Varandas, J. Phys. Chem. A 115 (2011) 7882–7890, https://doi.org/10.1021/jp2032912.
[18] D. Herraez-Aguilar, P.G. Jambrina, M. Menendez, J. Aldegunde, R. Warmbier, F. J. Aoiz, Phys. Chem. Chem. Phys. 16 (2014) 24800–24812, https://doi.org/10.1039/C4CP03289F.
[19] S. Rampino, M. Pastore, E. Garcia, A. Laganà, L. Pacifici, Mon. Not. R. Astron. Soc. 460 (2016) 2368–2375, https://doi.org/10.1093/mnras/stw1116.
[20] L. Pacifici, M. Pastore, E. Garcia, A. Laganà, S. Rampino, J. Phys. Chem. A 120 (2016) 5125–5135, https://doi.org/10.1021/acs.jpca.6b00564.
[21] H. Song, A. Li, M. Yang, H. Guo, Phys. Chem. Chem. Phys. 19 (2017) 17396–17403, https://doi.org/10.1039/C7CP02889J.
[22] P.G. Jambrina, F.J. Aoiz, N. Bulut, S.C. Smith, G.G. Balint-Kurti, M. Hankel, Phys. Chem. Chem. Phys. 12 (2010) 1102–1115, https://doi.org/10.1039/b919914d.
[23] P.G. Jambrina, J.M. Alvariño, F.J. Aoiz, V.J. Herrero, V. Sáez-Rábanos, Phys. Chem. Chem. Phys. 12 (2010) 12591–12603, https://doi.org/10.1039/C0CP00311E.
[24] P.G. Jambrina, J.M. Alvariño, D. Gerlich, M. Hankel, V.J. Herrero, V. Sáez-Rábanos, F.J. Aoiz, Phys. Chem. Chem. Phys. 14 (2012) 3346–3359. doi:10.1039/C2CP23479C.
[25] O. Denis-Alpizar, V.V. Guzmán, N. Inostroza, Mon. Not. R. Astron. Soc. 479 (2018) 753–757, https://doi.org/10.1093/mnras/sty1506.
[26] S. Gómez-Carrasco, L. González-Sánchez, A. Aguado, C. Sanz-Sanz, A. Zanchet, O. Roncero, J. Chem. Phys. 137 (2012) 094303, https://doi.org/10.1063/1.4747548.
[27] A. Zanchet, M. Agúndez, V.J. Herrero, A. Aguado, O. Roncero, Astron. J. 146 (2013) 125, https://doi.org/10.1088/0004-6256/146/5/125.
[28] A. Zanchet, F. Lique, O. Roncero, J.R. Goicoechea, N. Bulut, Astron. Astrophys. 626 (2019) A103, https://doi.org/10.1051/0004-6361/201935471.
[29] O. Martinez, S.G. Ard, A. Li, N.S. Shuman, H. Guo, A.A. Viggiano, J. Chem. Phys. 143 (2015) 114310, https://doi.org/10.1063/1.4931109.
[30] A. Zanchet, et al., Phys. Chem. Chem. Phys. 20 (2018) 5415–5426, https://doi.org/10.1039/C7CP05307J.
[31] O. Roncero, A. Zanchet, A. Aguado, Phys. Chem. Chem. Phys. 20 (2018) 25951–25958, https://doi.org/10.1039/C8CP04970J.
[32] E. Roueff, F. Lique, Chem. Rev. 113 (2013) 8906–8938, https://doi.org/10.1021/cr400145a.
[33] Y.V. Suleimanov, F.J. Aoiz, H. Guo, J. Phys. Chem. A 120 (2016) 8488–8502, https://doi.org/10.1021/acs.jpca.6b07140.
[34] S. Rampino, Y.V. Suleimanov, J. Phys. Chem. A 120 (2016) 9887–9893, https://doi.org/10.1021/acs.jpca.6b10592.
[35] Y.V. Suleimanov, A. Aguado, S. Gómez-Carrasco, O. Roncero, J. Phys. Chem. Lett. 9 (2018) 2133–2137, https://doi.org/10.1021/acs.jpclett.8b00783.
[36] S. Bhowmick, D. Bossion, Y. Scribano, Y.V. Suleimanov, Phys. Chem. Chem. Phys. 20 (2018) 26752–26763, https://doi.org/10.1039/C8CP05398G.
[37] S.S. Kumar, F. Grussie, Y.V. Suleimanov, H. Guo, H. Kreckel, Sci. Adv. 4 (2018) eaar3417, https://doi.org/10.1126/sciadv.aar3417.
[38] D. Nuñez-Reyes, K.M. Hickson, P. Larrégaray, L. Bonnet, T. González-Lezana, S. Bhowmick, Y.V. Suleimanov, Phys. Chem. Chem. Phys. 20 (2018) 4404–4414, https://doi.org/10.1039/C7CP07843A.
[39] P. del Mazo-Sevillano, A. Aguado, E. Jiménez, Y.V. Suleimanov, O. Roncero, J. Phys. Chem. Lett. 10 (2019) 1900–1907, https://doi.org/10.1021/acs.jpclett.9b00555.
[40] D. Nuñez-Reyes, K.M. Hickson, P. Larrégaray, L. Bonnet, T. González-Lezana, S. Bhowmick, Y.V. Suleimanov, J. Phys. Chem. A 123 (2019) 8089–8098, https://doi.org/10.1021/acs.jpca.9b06133.
[41] M. Menéndez, P.G. Jambrina, A. Zanchet, E. Verdasco, Y.V. Suleimanov, F.J. Aoiz, J. Phys. Chem. A 123 (2019) 7920–7931, https://doi.org/10.1021/acs.jpca.9b06695.
[42] T. González-Lezana, D. Bossion, Y. Scribano, S. Bhowmick, Y.V. Suleimanov, J. Phys. Chem. A 123 (2019) 10480–10489, https://doi.org/10.1021/acs.jpca.9b06122.
[43] W.L. Hase, R.J. Duchovic, X. Hu, A. Komornicki, K.F. Lim, D. Lu, G.H. Peslherbe, K. N. Swamy, S.R. van de Linde, A.J.C. Varandas, H. Wang, R.J. Wolf, VENUS96: A general chemical dynamics computer program, 1996.
[44] K. Haris, A. Kramida, Astrophys. J., Suppl. Ser. 233 (2017) 16, https://doi.org/10.3847/1538-4365/aa86ab.

[45] R.D.L. Levine, R.B. Bernstein, Molecular Reaction Dynamics and Chemical Reactivity, Oxford University Press, 1987, https://doi.org/10.1017/CBO9780511614125.
[46] J. Israelachvili, Intermolecular and Surface Forces, Academic Press, 2011.
[47] T.M. Miller, B. Bederson, volume 13 of Adv. At. Mol. Phys., Academic Press, 1978, pp. 1–55. doi:10.1016/S0065-2199(08)60054-8.
[48] E.A. Scarl, F.W. Dalby, Can. J. Phys. 52 (1974) 1429–1437, https://doi.org/10.1139/p74-190.
[49] D.M. Kooij, Z. Phys, Chem, Abt. B 12 (1893) 155–161.